THE JOURNAL OF PHYSICAL CHEMISTRY A

Article

pubs.acs.org/JPCA

Activation Strain Analysis of S_N2 Reactions at C, N, O, and F Centers

Jan Kubelka[†] and F. Matthias Bickelhaupt[*,‡,§]

[†]Department of Chemistry, University of Wyoming, Laramie, Wyoming 82070, United States

[‡]Department of Theoretical Chemistry and Amsterdam Center for Multiscale Modeling (ACMM), Vrije Universiteit Amsterdam, De Boelelaan 1083, 1081 HV Amsterdam, The Netherlands

[§]Institute for Molecules and Materials (IMM), Radboud University, Heyendaalseweg 135, 6525 AJ Nijmegen, The Netherlands

Supporting Information

ABSTRACT: Fundamental principles that determine chemical reactivity and reaction mechanisms are the very foundation of chemistry and many related fields of science. Bimolecular nucleophilic substitutions (S_N2) are among the most common and therefore most important reaction types. In this report, we examine the trends in the S_N2 reactions with respect to increasing electronegativity of the reaction center by comparing the well-studied backside S_N2 $Cl^- + CH_3Cl$ with similar Cl^- substitutions on the isoelectronic series with the second period elements N, O, and F in place of C. Relativistic (ZORA) DFT calculations are used to construct the gas phase reaction potential energy surfaces (PES), and activation strain analysis, which allows decomposition of the PES into the geometrical strain and interaction energy, is employed to analyze the observed trends. We find that S_N2@N and S_N2@O have similar PES to the prototypical S_N2@C, with the well-defined reaction complex (RC) local minima and a central barrier, but all stationary points are, respectively, increasingly stable in energy. The S_N2@F, by contrast, exhibits only a single-well PES with no barrier. Using the activation strain model, we show that the trends are due to the interaction energy and originate mainly from the decreasing energy of the empty acceptor orbital (σ^*_{A-Cl}) on the reaction center A in the order of C, N, O, and F. The decreasing steric congestion around the central atom is also a likely contributor to this trend. Additional decomposition of the interaction energy using Kohn–Sham molecular orbital (KS-MO) theory provides further support for this explanation, as well as suggesting electrostatic energy as the primary reason for the distinct single-well PES profile for the FCl reaction.

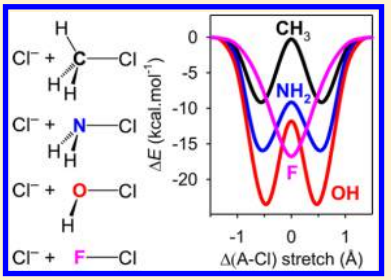

1. INTRODUCTION

Understanding chemical reactions and reactivity is one of the central goals of chemistry and, more broadly, all natural science. The ability of molecular species to react and form new, more complex ones is responsible for the evolution and existence of the Universe, Earth, and biological life.[1] In modern society, design and production of new compounds and materials[2,3] is key for technological advances that help sustain the growing and expanding human population. Fundamental insights into the underlying physical principles behind key chemical processes are therefore critical for further progress in their future development, control, and optimization.

One of the most important prototypes of chemical reactions is bimolecular nucleophilic substitution (S_N2, see Scheme 1).[4] Due to its significance, numerous experimental and theoretical studies have been focused on providing detailed, fundamental understanding of the S_N2 reactions.[5−22] Perhaps the best-known model for S_N2 reactions is the symmetric, thermoneutral S_N2 reaction between the chloride anion and chloromethane, $Cl^- + CH_3Cl$ in the gas phase (Scheme 1).

This reaction proceeds preferentially through backside nucleophilic attack of the chloride anion at the carbon atom (S_N2@C) with concerted expulsion of the leaving group. A well-known feature of gas phase S_N2@C reactions is their double-well potential energy surface (PES) along the reaction coordinate,[5] as illustrated in Figure 1. This PES is characterized by a central barrier, provided by a trigonal bipyramidal transition state (TS, see also Scheme 1), that separates two energy minima, associated with the reactant and product ion–molecule complexes (RC and PC).

Scheme 1. Archetypal S_N2 Reaction

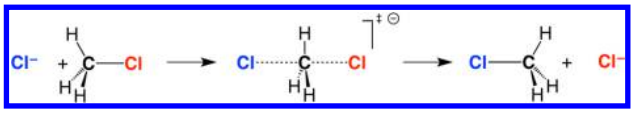

Among the most powerful approaches to understanding reactivity is examining trends with respect to some selected properties of the reacting species. Although many trends could be explained using chemical intuition or empirical understanding, when combined with modern quantum chemical calculations it is possible to uncover the details of the electronic structure and its changes associated with the observed trends, thereby providing the fundamental explanations. Bento and Bickelhaupt recently used relativistic DFT calculations together with analysis by the activation strain model[6,23−27] to examine

Received: December 5, 2016
Revised: December 22, 2016
Published: January 3, 2017

DOI: 10.1021/acs.jpca.6b12240
J. Phys. Chem. A 2017, 121, 885−891

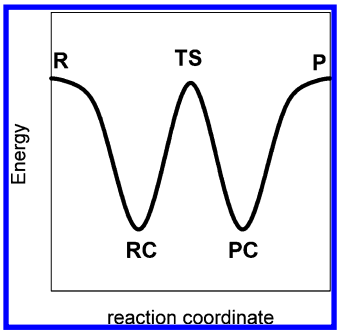

Figure 1. Schematic potential energy surface (PES) for an S_N2 reaction. R stands for reactants, RC for reaction complex, TS for transition state, PC for product complex, and P for products.

the effects of the nucleophile and the leaving group on methyl chloride (CH_3Cl) S_N2 reactions, both backside and frontside.[18] This study demonstrated that the nucleophilicity is determined by the electron-donor capability of the nucleophile, while the leaving group ability is associated primarily with the carbon−leaving group bond strength.

The same authors also investigated the S_N2 reactions according to Scheme 1 with the central C atom substituted by heavier group-14 atoms (Si, Ge, Sn, Pb). An interesting feature of the PES for the S_N2@Si, @Ge, @Sn, and @Pb reactions is that the central barrier disappears, giving rise to a single-well reaction profile.[19,20] They showed that the disappearance of the central barrier is due to the decrease in steric repulsion for the larger atoms along with more stabilizing orbital interactions due to better chloride HOMO/substrate LUMO overlap.[19]

The next level of the quest for a more complete understanding of the S_N2 reactions is the examination of trends with respect to substitutions on atoms other than carbon and its group-14 congeners. Several theoretical reports compare various aspects of S_N2@C reactions to S_N2@N,[7−11,21] S_N2@P,[13−16] S_N2@O,[12,21] and S_N2@S.[21] However, these studies often focus on thermochemistry,[7,12] molecular geometries,[7−9] effects of different nucleophiles and/or leaving groups,[7,8,11−14,21] solvation,[15] or comparison of different computational methods,[9,10,21] and few seek a systematic examination of trends with respect to the properties of the central atom and their significance in the S_N2 reactivity.[13,16] Here we take the first step in this direction by considering on the S_N2 reactions for all substrates of the second period elements that are isoelectronic to the CH_3Cl prototype, namely, NH_2Cl, OHCl, and FCl (Scheme 2). This series provides a potentially very rich model set for understanding the roles of several key factors in the S_N2 reactivity that may be furthermore representative of the corresponding groups of the periodic table. In particular, there is a strong trend of increasing electronegativity from C to F which goes with a more negatively charged electrophilic central atom. Intuitively, one might expect that higher electronegativity will lead to higher barriers due to repulsion with the approaching nucleophile. On the other hand, the valence of the central element decreasing in the same order results in different geometry of the reacting species and transition states, which may manifest itself via geometry strain and steric effects. The resulting PESs are therefore expected to reflect, to a greater or lesser extent, an interplay of both these fundamental contributions. To sort out the roles of each of these individual PES components, we take advantage of the activation strain model,[6,26,27] which has been specifically designed for this purpose (see Methods for details), and use this powerful methodology to identify the underlying physical reasons and explanations for the observed trends in the S_N2 reactivity.

Scheme 2. Model S_N2@element Reactions Analyzed in This Work

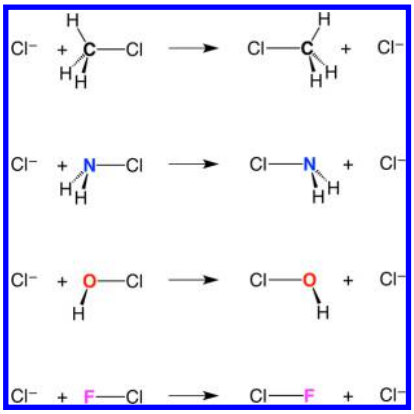

2. METHODS

2.1. Computational Details. All calculations were performed with the Amsterdam Density Functional (ADF) program.[28−30] The molecular orbitals (MOs) were expanded in a large uncontracted set of Slater-type orbitals (STOs) containing diffuse functions, TZ2P.[29,30] This basis is of triple-ζ quality and has been augmented by two sets of polarization functions: 2p and 3d on hydrogen and 3d and 4f on all heavier atoms. An auxiliary set of s, p, d, f, and g STOs was used to fit the molecular density and to represent the Coulomb and exchange potentials accurately in each SCF cycle. Relativistic effects were accounted for explicitly using the zeroth-order regular approximation (ZORA).[31] In our type of model reactions, relativity affects barriers by only a few tenths of a kcal/mol, or less.[19] Nevertheless, they were included to make this study technically consistent with earlier work.[18−20]

Equilibrium and transition-state geometries were fully optimized employing the OLYP[32,33] density functional, which involves Handy's optimized exchange, OPTX.[33] This level of theory was previously shown to agree satisfactorily with highly correlated *ab initio* benchmarks.[34−38] All stationary points were confirmed by vibrational analysis:[39] for equilibrium structures all normal modes have real frequencies whereas transition states have one normal mode with an imaginary frequency.[40] Transition states were verified to connect the supposed educt and product minima by carrying out intrinsic reaction coordinate (IRC) calculations.[41]

2.2. Analysis of the Potential Energy Surfaces. Insight into how the activation barriers arise is obtained through activation strain analyses of the various S_N2 reactions. The activation strain model[6,23−27] (also known as distortion/interaction model)[42,43] is a fragment approach to understanding chemical reactions, in which the height of reaction barriers is described in terms of the original reactants. Thus, the potential energy surface $\Delta E(\zeta)$ is decomposed, along the reaction coordinate ζ, into the strain $\Delta E_{strain}(\zeta)$ associated with deforming the individual reactants plus the actual interaction $\Delta E_{int}(\zeta)$ between the deformed reactants:

$$\Delta E(\zeta) = \Delta E_{strain}(\zeta) + \Delta E_{int}(\zeta) \quad (1)$$

DOI: 10.1021/acs.jpca.6b12240
J. Phys. Chem. A 2017, 121, 885−891

The strain $\Delta E_{strain}(\zeta)$ is determined by the rigidity of the reactants and by the extent to which groups must reorganize in a particular reaction mechanism, whereas the interaction $\Delta E_{int}(\zeta)$ between the reactants depends on their electronic structure and on how they are mutually oriented as they approach each other. It is the interplay between $\Delta E_{strain}(\zeta)$ and $\Delta E_{int}(\zeta)$ that determines if and at which point along the ζ a barrier arises. The activation energy of a reaction $\Delta E^{\ddagger} = \Delta E(\zeta^{TS})$ consists of the activation strain $\Delta E^{\ddagger}_{strain} = \Delta E_{strain}(\zeta^{TS})$ plus the TS interaction $\Delta E^{\ddagger}_{int} = \Delta E_{int}(\zeta^{TS})$:

$$\Delta E^{\ddagger} = \Delta E^{\ddagger}_{strain} + \Delta E^{\ddagger}_{int} \quad (2)$$

In the graphical representations shown below, ζ is then projected onto the stretch of the central atom−leaving group (A−Cl, A = C, N, O, and F) bond, which is generally one of the dominant components of the reaction coordinate and undergoes a well-defined change from an intact to a dissociated bond.

The interaction $\Delta E_{int}(\zeta)$ between the strained reactants is further analyzed in the conceptual framework provided by the Kohn−Sham molecular orbital (KS-MO) model,[44−49] according to which it is decomposed into three physically meaningful terms:

$$\Delta E_{int}(\zeta) = \Delta V_{elstat}(\zeta) + \Delta E_{Pauli}(\zeta) + \Delta E_{oi}(\zeta) \quad (3)$$

The term ΔV_{elstat} corresponds to the classical electrostatic interaction between the unperturbed charge distributions of the deformed reactants and is usually attractive. The Pauli repulsion ΔE_{Pauli} comprises the destabilizing interactions between occupied orbitals and is responsible for any steric repulsion (see ref. 44 for an exhaustive discussion). The orbital interaction ΔE_{oi} accounts for charge transfer (interaction between occupied orbitals on one moiety with unoccupied orbitals of the other, including HOMO−LUMO interactions) and polarization (empty−occupied orbital mixing on one fragment due to the presence of another fragment).

The activation strain analysis was performed with the aid of the PyFrag program[50] at discrete points on the reaction coordinate, sampled from the computed IRC paths (see above), except Cl^- + FCl, where due to the absence of a TS a relaxed energy scan (linear transit) along the F−Cl bond was used.

3. RESULTS AND DISCUSSION

3.1. Reaction Profiles. The computed energies of the reaction complexes (RC), transition states (TS), and transition complex (TC) with respect to the free reactants are summarized in Table 1. Also shown in Table 1 are the A−Cl^- distances (where A stands for the central atom; A = C, N, O, F) at the respective stationary points. The corresponding reaction profiles are superimposed in Figure 2. Our ZORA-OLYP/TZ2P computations show that all the model reactions proceed via a Cl−A−Cl symmetric transition structure which is either a labile transition state (for A = C, N, O) or a stable intermediate transition complex (for A = F). Furthermore, there is a systematic trend in the energy of this symmetric TS or TC relative to the reactants: along A = C, N, O, and F, it decreases from −0.3 to −9.2 to −11.3 to −16.8 kcal·mol^{-1}, respectively (Table 1).

Table 1. Relative Energies (in kcal·mol^{-1}) and Geometries (in Å) for the Stationary Points along the Cl^- + AH_nCl S_N2 Reactions[a]

	CH_3Cl	NH_2Cl	OHCl	FCl
ΔE (RC)	−9.2	−15.9	−23.5	
ΔE (TS)[a]	−0.3	−9.2	−11.3	
ΔE (TC)[a]				−16.8
A−Cl (R)[a]	1.790	1.766	1.711	1.654
A−Cl (RC)	1.835	1.786	1.705	
A−Cl (TS)	2.351	2.286	2.176	
A−Cl (TC)				2.085

[a]Computed at ZORA-OLYP/TZ2P. R = reactants; RC = reaction complex; TS = transition state, TC = transition complex (for FCl).

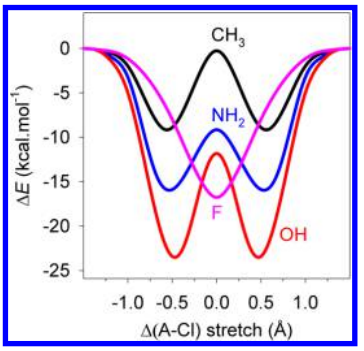

Figure 2. Potential energy surfaces relative to free reactants of the S_N2 reactions of Cl^- + AH_nCl with AH_n = CH_3, NH_2, OH, and F, computed at ZORA-OLYP/TZ2P. The reaction coordinate (horizontal axis) is defined as the Nu−A and A−LG stretch with respect to the TS (Nu = nucleophile, LG = leaving group).

The Cl^- + CH_3Cl reaction exhibits the characteristic double-well PES involving local minima corresponding to the reaction complexes (RC) and a central barrier for the transition state (TS), in line with previous studies.[5,17−19,51] The energy profiles for NH_2Cl and OHCl reactions are qualitatively similar, but significantly lower in energy (Table 1). Specifically, the RCs are respectively 7 and 25 kcal·mol^{-1} lower, while the TSs are 9 and 23 kcal·mol^{-1} below the computed values for the CH_3Cl + Cl^- substitution (all values relative to the reactants). The height of the reaction barrier with respect to the RC, however, does not follow the same trend. It is computed to be 9, 7, and 12 kcal·mol^{-1} for the reactions with CH_3Cl, NH_2Cl, and OHCl, respectively.

By contrast, the Cl^- + FCl reaction profile is qualitatively different, with only a single minimum corresponding to the symmetric $[Cl−F−Cl]^-$ transition complex and no separate, asymmetric RC. The TC is stable by 17 kcal·mol^{-1} compared to the individual reactants (Table 1). This species features a strong halogen bond and electron-rich hypervalent fluorine.[52] Similar single-well profiles were identified for S_N2 substitutions on heavier group-14 atoms: Si, Ge, Sn, and Pb.[19] In fact, under certain conditions, they may also exist for S_N2 substitution on carbon.[53]

Another trend apparent from Table 1 is the systematic decrease in bond distances between the central atom and the Cl^- leaving group for both RC and transition structure (TS or TC) in the order C, N, O, and F. The differences are somewhat greater for the TS (by ∼0.02 Å) and also decrease more significantly from S_N2@N to S_N2@O than from S_N2@C to S_N2@N, by about 0.04 Å for both RC and TS. The trend continues for the S_N2 substitution at F although, as mentioned above, no asymmetric RC exists, only a stable TC. In this stable $[Cl−F−Cl]^-$ complex the F−Cl bond lengths are greater than in the RCs for the other compounds. However, when compared

DOI: 10.1021/acs.jpca.6b12240
J. Phys. Chem. A 2017, 121, 885−891

to the TS, the bond again shortens from O−Cl to F−Cl (Table 1).

For completeness, in Table 2 we present the thermochemistry activation parameters for the studied reactions, calculated for 1 atm, 298.15 K. The trends in the activation thermodynamic energy (i.e., electronic energy plus ZPVE plus thermal energy of translation, rotation, and vibration) and enthalpy parallel the electronic energy presented in Table 1. All $\Delta H^{\ddagger}$ are negative, implying that the reaction rates would exhibit an anti-Arrhenius behavior in the gas phase, i.e., they would decrease with the increasing temperature. The activation entropy (given as $-T\Delta S^{\ddagger}$) is essentially constant for CH_3Cl, NH_2Cl, and OHCl reactions, and only 1 kcal·mol^{-1} lower for the FCl, yielding quantitatively very similar progression in the activation Gibbs free energies. Note, however, that there is a qualitative difference: the $\Delta G^{\ddagger}$ for the Cl^- + CH_3Cl reaction is slightly positive, therefore presenting an actual activation barrier, while all others are negative. Thus, at low-pressure conditions, the gas-phase S_N2 substitution at C still experiences an entropy bottleneck whereas gas-phase S_N2 substitution at N, O, and F proceeds spontaneously. Note that at higher pressure, as energy dissipation becomes important, the central barrier (i.e., relative to the RC or TC) becomes decisive.

Table 2. Thermochemistry of Activation (in kcal·mol^{-1}) for the Studied S_N2 Reactions[a]

	Cl^- + CH_3Cl	Cl^- + NH_2Cl	Cl^- + OHCl	Cl^- + FCl
$\Delta U^{\ddagger}$	−0.6	−9.6	−12.5	−16.3
$\Delta H^{\ddagger}$	−1.2	−10.2	−13.1	−16.9
$-T\Delta S^{\ddagger}$	7.5	7.5	7.6	6.5
$\Delta G^{\ddagger}$	6.3	−2.7	−5.5	−10.4

[a]Computed at ZORA-OLYP/TZ2P for 1 atm, 298.15 K.

At first sight, the mechanism behind the above trends may not be entirely obvious. Why should the relative energy of the TS or TC go down, if the nucleophile attacks a more electronegative and thus more negatively charged (*vide infra*) central atom if one goes from A = C to A = N, O, and F? On the other hand, intuitively, a more electronegative central atom may also be conceived more electrophilic and prone to interact with the lone pair of an incoming nucleophile. As pointed out above, however, there may be yet another important contribution to the energetics and, consequently, shapes of the PES, from the structural strain. In the next section we employ the activation strain model to analyze the various S_N2 reaction profiles and provide sound physical explanations for the observed trends.

3.2. Activation Strain Analyses. As detailed in Methods, the activation strain analysis[6,23−25] decomposes the total $\Delta E(\zeta)$ of the model reactions along the reaction coordinate ζ, into the strain $\Delta E_{strain}(\zeta)$ component associated with deforming the individual reactants plus the actual interaction $\Delta E_{int}(\zeta)$ between the deformed reactants. The analysis results of the studied reactions are presented in Figures 3 and 4. Figure 3 shows the activation strain diagrams for each particular reaction, while Figure 4 overlays the strain $\Delta E_{strain}(\zeta)$ (Figure 3a) and interaction $\Delta E_{int}(\zeta)$ (Figure 3b) energies for direct comparison. For easier reference the positions of the transition states are also indicated.

It is evident from both Figures 3 and 4, but perhaps more from the latter, that the observed trends in the PES profiles are associated mostly with the interaction energy (Figure 4b)

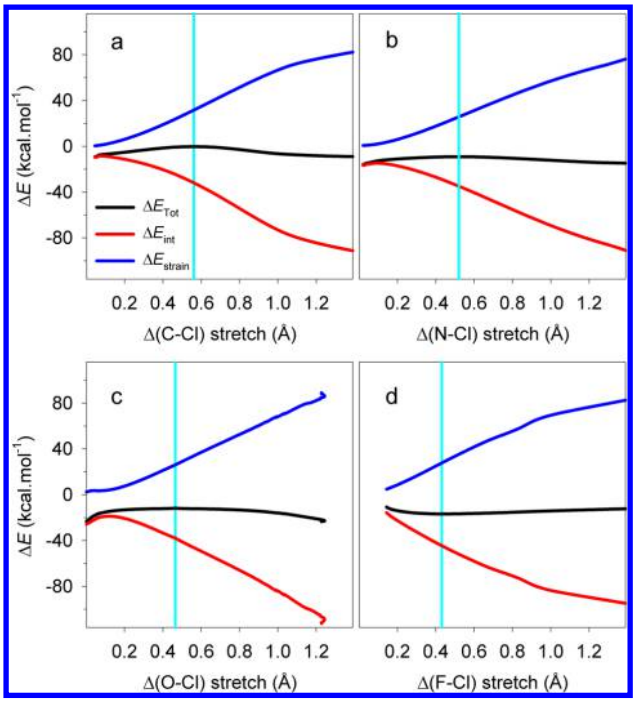

Figure 3. Activation strain analysis of the S_N2 reaction profiles. Total energy (black), decomposed into strain (blue) and interaction (red) components plotted as a function of the A−Cl stretch coordinate with respect to its equilibrium value for (a) Cl^- + CH_3Cl reaction (A = C), (b) Cl^- + NH_2Cl reaction (A = N), (c) Cl^- + OHCl reaction (A = O), and (d) Cl^- + FCl reaction (A = F). The pale blue vertical lines indicate the position of the transition state.

rather than the strain (Figure 4a). In Table 3, we list the values of the ΔE_{strain} and ΔE_{int} at the TS or, for SN2@F, TC. Although the strain energy does destabilize the TS of the Cl^- + CH_3Cl with respect to NH_2Cl and OHCl ones by ∼5 kcal·mol^{-1}, the latter two have virtually the same TS strain energy and the Cl^- + FCl reaction complex has again slightly higher strain, counter to the progression in the total energy (Figure 2). These differences in the ΔE_{strain} correlate well with the order of A−Cl bond dissociation energies, that is, stronger bonds go with more destabilizing strain curves (Table 4).[19]

By contrast, the interaction energies (Figure 4b, see also Table 3) show a very clear trend of stabilization in the order of C, N, O, F. The explanation can be found from the examination of the dominant frontier orbital interaction between the occupied Cl^- 3p AO and the backside lobe of the empty σ^*_{A-Cl} orbital.[19] As shown in Table 4, the σ^*_{A-Cl} energy monotonically decreases with the increasing electronegativity of the central atom, respectively, for along C, N, O, and F. This reflects the decreasing orbital energy of the central atom's 2p AOs in this order. The monotonic decrease of the σ^*_{A-Cl} orbital energy along CH_3Cl, NH_2Cl, OHCl, and FCl causes the HOMO−LUMO gap $\Delta\varepsilon$ between nucleophile Cl^- 3p AO and substrate σ^*_{A-Cl} to become smaller and thus the orbital interactions to become more stabilizing. This is what we see in the systematic trend in interaction curves, in perfect agreement with the relationship $\Delta E_{oi} \sim S^2/\Delta\varepsilon$, where S represents the overlap integral (Table 4) and $\Delta\varepsilon$ is the energy difference between the interacting orbitals.[44] Note that the orbital overlap, shown in Table 4 for the TS (TC), decreases slightly with the increasing electronegativity of A (with the exception of N and O), consistently with the generally greater wave function

DOI: 10.1021/acs.jpca.6b12240
J. Phys. Chem. A 2017, 121, 885−891

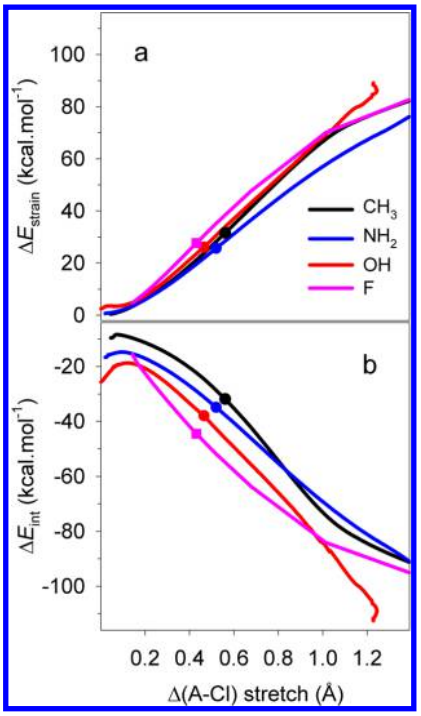

Figure 4. Comparison of the strain and interaction energies for the studied S_N2 reactions. (a) Strain energy and (b) interaction energy plotted as a function of the A−Cl stretch coordinate with respect to its equilibrium value for Cl^- + CH_3Cl reaction (black lines), Cl^- + NH_2Cl reaction (red lines), Cl^- + OHCl reaction (blue lines), and Cl^- + FCl reaction (pink lines). The solid circles indicate the positions of the transition states, the pink square for Cl^- + FCl the position of the transition complex.

Table 3. Activation Strain Analysis (in kcal·mol^{-1}) at the TS of the Studied S_N2 Reactions[a]

	Cl^- + CH_3−Cl	Cl^- + NH_2−Cl	Cl^- + OH−Cl	Cl^- + F−Cl
$\Delta E^{\ddagger}$	−0.3	−9.2	−11.8	−16.8
$\Delta E^{\ddagger}_{strain}$	31.6	25.7	26.1	27.7
$\Delta E^{\ddagger}_{int}$	−31.9	−34.9	−37.9	−44.5

[a]Computed at the ZORA-OLYP/TZ2P level.

Table 4. Properties of the Substrates in Studied S_N2 Reactions: A−Cl Bond Strengths (in kcal·mol^{-1}), σ^*_{A-Cl} Orbital Energy (in eV), and A Atomic Charge (in au)[a]

	CH_3−Cl	NH_2−Cl	OH−Cl	F−Cl
BDE[b]	−84.2	−63.4	−58.6	−65.3
σ^*_{A-Cl}	−5.13	−6.96	−8.95	−11.08
$Q^{VDD}(A)$[c]	−0.031	−0.143	−0.152	−0.072
Δen[d]	−0.61	−0.12	0.28	0.82
S[e]	0.215	0.174	0.183	0.131

[a]Computed at ZORA-OLYP/TZ2P. [b]Bond dissociation energy. [c]VDD atomic charge.[54] [d]Pauling electronegativity difference of central atom relative to Cl.[55] [e]Overlap integral between HOMO (3p) of Cl^- and LUMO (σ^*_{A-Cl}) of each substrate at the TS (TC).

amplitude on the more electropositive element of the A−Cl bond, which opposes the stabilization effect of the HOMO−LUMO gap. The $\Delta\varepsilon$ is therefore clearly the decisive factor in determining the interaction energy, as evidenced particularly by the greatest amount of stabilization in F−Cl (Figure 4b, Table 4).

That the orbital interaction is indeed the dominant contribution to the ΔE_{int} trend is further confirmed by the examination of the decomposition of ΔE_{int} according to our quantitative analysis associated with the KS-MO model[44−49] (see Methods). The individual components, ΔE_{Pauli}, ΔV_{elstat}, and ΔE_{oi}, are overlaid for all four studied S_N2 reactions in Figure 5. Both the Pauli repulsion term (ΔE_{Pauli}, Figure 5a) and

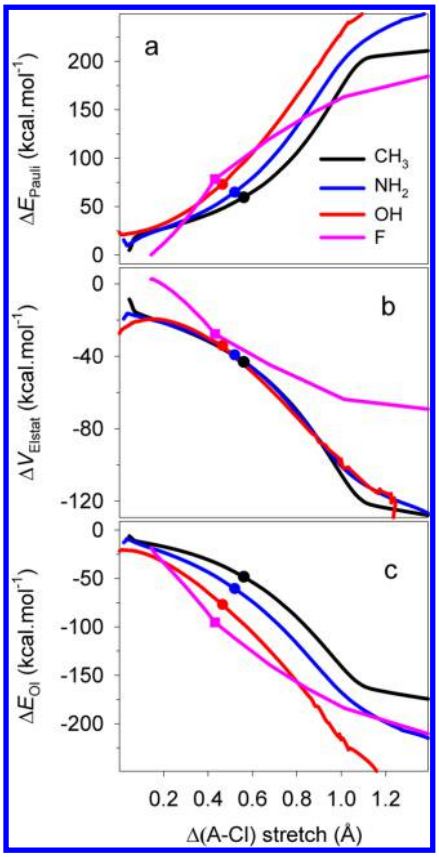

Figure 5. Kohn−Sham molecular orbital (KS-MO) analysis of the interaction energies for the studied S_N2 reactions. (a) Pauli repulsion energy, (b) electrostatic interaction energy, and (c) orbital interaction energy plotted as a function of the A−Cl stretch coordinate with respect to its equilibrium value for Cl^- + CH_3Cl reaction (black lines), Cl^- + NH_2Cl reaction (red lines), Cl^- + OHCl reaction (blue lines), and Cl^- + FCl reaction (pink lines). The solid circles indicate the positions of the transition states, the pink square for Cl^- + FCl the position of the stable transition complex.

the electrostatic interaction (ΔV_{elstat}, Figure 5b) oppose the trend; although the $\Delta V_{elstat}(\zeta)$ curves appear nearly superimposable, the shifted TS positions in fact result in less stabilizing $\Delta V_{elstat}(\zeta^{TS})$ contributions from C to N, O, and F. The ΔE_{oi} (Figure 5c) is the only term that decreases in this order and, thanks to its magnitude (note different scales on the Figure 5 panels), results in the overall progression of the ΔE_{int}.

Another factor that may possibly contribute to the computed trends in the ΔE_{int} for the studied series of the S_N2 reactions is the diminishing steric congestion around the reaction center due to the fewer substituent hydrogen atoms in CH_3Cl, NH_2Cl, OHCl, and FCl, respectively. In earlier, detailed analyses, the combination of more favorable steric effects and orbital interactions was found to be responsible for the disappearance of the central barrier in S_N2@Si as well as heavier group-14 atoms.[19] Furthermore, Pierrefixe et al. explicitly tested the role

DOI: 10.1021/acs.jpca.6b12240
J. Phys. Chem. A 2017, 121, 885−891

of the steric congestion by hydrogens bound to the central carbon for a series of Cl^--induced S_N2@C reactions with CH_3Cl, $CH_2Cl^•$, $CHCl^{••}$, and $CCl^{•••}$,[56] which have the same number of central atom bound hydrogens as our model series. They found that the central activation barrier becomes systematically lower with the decreasing number of hydrogens bound to the central atom and vanishes completely for the $CCl^{•••}$, paralleling our result for S_N2@F.

Finally, the difference in shape between the PES for S_N2@C, S_N2@N, and S_N2@O and that for S_N2@F is also codetermined by the strength of the hydrogen bonds that promote the occurrence of a stable RC and PC. Note that the relative energy of the S_N2@F TC complex exactly fits the trend of the TS energetics for the other reactions: the symmetric TS or TC systematically decreases in energy relative to separate reactants along C, N, O, and F. However, the central barrier, that is, the TS energy relative to the RC energy, behaves less systematically. This is because it is dependent not only on the trend in stability of the symmetric transition species (TS or TC) but also on the stability or even the availability of the $Cl^-\cdots H-AH_{n-1}Cl$ hydrogen bond in the RC or PC. This hydrogen bond becomes stronger as the H−A bond becomes more polar, along $Cl^-\cdots H-CH_2Cl$, $Cl^-\cdots H-NHCl$, and $Cl^-\cdots H-OCl$ (see Table 1 and Figure 2). The hydrogen bonding in the RC (and PC) for S_N2@N and S_N2@O is evident from the geometries where, in contrast to the RC for S_N2@C, the Cl^- clearly aligns with the N−H or O−H bond. This pronounced H-bonding interaction is reflected also in the distinct downward curvature of the ΔE_{int} (Figure 4b) below d(A−Cl) of ∼0.1 Å for S_N2@N and S_N2@O. But it ceases to exist as soon as there is no hydrogen-bond donor anymore, namely, for FCl; and so vanishes the RC and PC in the case of S_N2@F.

4. CONCLUSIONS

The analyses of the S_N2 reactions of Cl^- + CH_3Cl, NH_2Cl, OHCl, and FCl based on relativistic density functional theory reveal a consistent trend, whereby the overall reaction barriers are progressively lower in energy with the increasing electronegativity of the reaction center. The reaction complexes (RC) likewise become increasingly stabilized the more electronegative the central atom, with the exception of FCl, which yields a single-well PES with no central barrier.

Analyses based on the activation strain model show that the trend is entirely due to the increasingly stabilizing interaction energy between nucleophile and substrate, with minimal contribution from the geometric strain. The origin of this trend lies predominantly (although not exclusively) in the lower energy of the unoccupied acceptor orbital (σ^*_{A-Cl}) as the electronegativity of the substitution center A (= C, N, O, and F) increases. This σ^*_{A-Cl} orbital-energy lowering leads to a stronger HOMO−LUMO orbital interaction with the 3p lone-pair orbital of the Cl^- nucleophile.

These results underline the importance of the reaction center electronegativity and orbital interactions in shaping the S_N2 reaction profiles. They also demonstrate the great utility of relativistic DFT calculations and activation strain analyses for understanding the fundamentals of chemical reaction mechanisms.

■ ASSOCIATED CONTENT

Supporting Information

The Supporting Information is available free of charge on the ACS Publications website at DOI: 10.1021/acs.jpca.6b12240.

Cartesian coordinates, total ADF energies, and numbers of imaginary frequencies computed for all the species at stationary points of the studied reactions (PDF)

■ AUTHOR INFORMATION

Corresponding Author

*Fax: +31-20-59 87629. E-mail: FM.Bickelhaupt@vu.nl.

ORCID

F. Matthias Bickelhaupt: 0000-0003-4655-7747

Notes

The authors declare no competing financial interest.

■ ACKNOWLEDGMENTS

We thank The Netherlands Organization for Scientific Research (NWO-CW and NWO-EW) and NWO's Planetary and Exoplanetary Sciences (PEPSci) Program for financial support.

■ REFERENCES

(1) Francis, B. The Hypothesis That the Genetic Code Originated in Coupled Synthesis of Proteins and the Evolutionary Predecessors of Nucleic Acids in Primitive Cells. *Life* **2015**, *5*, 467−505.

(2) Grimsdale, A. C.; Mullen, K. The Chemistry of Organic Nanomaterials. *Angew. Chem., Int. Ed.* **2005**, *44*, 5592−5629.

(3) Langer, R.; Tirrell, D. A. Designing Materials for Biology and Medicine. *Nature* **2004**, *428*, 487−492.

(4) Smith, M. *March's Advanced Organic Chemistry*, 7th ed.; Wiley: Hoboken, NJ, 2013.

(5) Olmstead, W. N.; Brauman, J. I. Gas-Phase Nucleophilic Displacement Reactions. *J. Am. Chem. Soc.* **1977**, *99*, 4219−4228.

(6) Bickelhaupt, F. M. Understanding Reactivity with Kohn-Sham Molecular Orbital Theory: E2-S_N2 Mechanistic Spectrum and Other Concepts. *J. Comput. Chem.* **1999**, *20*, 114−128.

(7) Bühl, M.; Schaefer, H. F. S_N2 Reaction at Neutral Nitrogen - Transition-State Geometries and Intrinsic Barriers. *J. Am. Chem. Soc.* **1993**, *115*, 9143−9147.

(8) Bühl, M.; Schaefer, H. F. Theoretical Characterization of the Transition Structure for an S_N2 Reaction at Neutral Nitrogen. *J. Am. Chem. Soc.* **1993**, *115*, 364−365.

(9) Liu, X.; Zhang, J.; Yang, L.; Sun, R. Theoretical Studies on F^- + NH_2Cl Reaction: Nucleophilic Substitution at Neutral Nitrogen. *J. Phys. Chem. A* **2016**, *120*, 3740−3746.

(10) Yu, F. Assessment of Ab Initio MP2 and Density Functionals for Characterizing the Potential Energy Profiles of the S_N2 Reactions at N Center. *J. Comput. Chem.* **2012**, *33*, 1347−1352.

(11) Ren, Y.; Wei, X.-G.; Ren, S.-J.; Lau, K.-C.; Wong, N.-B.; Li, W.-K. The Alpha-Effect Exhibited in Gas-Phase S_N2@N and S_N2@C Reactions. *J. Comput. Chem.* **2013**, *34*, 1997−2005.

(12) Ren, Y.; Wolk, J. L.; Hoz, S. A G2(+) Level Investigation of the Gas-Phase Identity Nucleophilic Substitution at Neutral Oxygen. *Int. J. Mass Spectrom.* **2002**, *220*, 1−10.

(13) van Bochove, M. A.; Swart, M.; Bickelhaupt, F. M. Nucleophilic Substitution at Phosphorus Centers (S_N2@P). *ChemPhysChem* **2007**, *8* (17), 2452−2463.

(14) van Bochove, M. A.; Swart, M.; Bickelhaupt, F. M. Stepwise Walden Inversion in Nucleophilic Substitution at Phosphorus. *Phys. Chem. Chem. Phys.* **2009**, *11*, 259−267.

(15) van Bochove, M. A.; Bickelhaupt, F. M. Nucleophilic Substitution at C, Si and P: How Solvation Affects the Shape of Reaction Profiles. *Eur. J. Org. Chem.* **2008**, *4*, 649−654.

(16) van Bochove, M. A.; Swart, M.; Bickelhaupt, F. M. Nucleophilic Substitution at Phosphorus (S_N2@P): Disappearance and Reappearance of Reaction Barriers. *J. Am. Chem. Soc.* **2006**, *128*, 10738−10744.

(17) Bickelhaupt, F. M.; Baerends, E. J.; Nibbering, N. M. M. The Effect of Microsolvation on E2 and S_N2 Reactions: Theoretical Study

of the Model System F^- + C_2H_5F + nHF. *Chem. - Eur. J.* **1996**, *2*, 196−207.
(18) Bento, A. P.; Bickelhaupt, F. M. Nucleophilicity and Leaving-Group Ability in Frontside and Backside S_N2 Reactions. *J. Org. Chem.* **2008**, *73*, 7290−7299.
(19) Bento, A. P.; Bickelhaupt, F. M. Frontside versus Backside S_N2 Substitution at Group 14 Atoms: Origin of Reaction Barriers and Reasons for Their Absence. *Chem. - Asian J.* **2008**, *3*, 1783−1792.
(20) Bento, A. P.; Bickelhaupt, F. M. Nucleophilic Substitution at Silicon (S_N2@Si) via a Central Reaction Barrier. *J. Org. Chem.* **2007**, *72*, 2201−2207.
(21) Ren, Y.; Chu, S. Y. Recent Development in the Study of S_N2 Reactions at Heteroatoms and Ion Pair Systems. *J. Theor. Comput. Chem.* **2006**, *5*, 121−140.
(22) Xie, J.; Otto, R.; Mikosch, J.; Zhang, J.; Wester, R.; Hase, W. L. Identification of Atomic-Level Mechanisms for Gas-Phase X^- + CH_3Y S_N2 Reactions by Combined Experiments and Simulations. *Acc. Chem. Res.* **2014**, *47*, 2960−2969.
(23) Diefenbach, A.; de Jong, G. T.; Bickelhaupt, F. M. Activation of H-H, C-H, C-C and C-Cl Bonds by Pd and $PdCl^-$. Understanding Anion Assistance in C-X Bond Activation. *J. Chem. Theory Comput.* **2005**, *1*, 286−298.
(24) Diefenbach, A.; Bickelhaupt, F. M. Oxidative Addition of Pd to C-H, C-C and C-Cl Bonds: Importance of Relativistic Effects in DFT Calculations. *J. Chem. Phys.* **2001**, *115*, 4030−4040.
(25) de Jong, G. T.; Bickelhaupt, F. M. Transition-State Energy and Position along the Reaction Coordinate in an Extended Activation Strain Model. *ChemPhysChem* **2007**, *8*, 1170−1181.
(26) Fernandez, I.; Bickelhaupt, F. M. The Activation Strain Model and Molecular Orbital Theory: Understanding and Designing Chemical Reactions. *Chem. Soc. Rev.* **2014**, *43*, 4953−4967.
(27) Wolters, L. P.; Bickelhaupt, F. M. The Activation Strain Model and Molecular Orbital Theory. *Wiley Interdiscip. Rev. Comput. Mol. Sci.* **2015**, *5*, 324−343.
(28) Baerends, E. J.; Ziegler, T.; Autschbach, J.; Bashford, D.; Bérces, A.; Bickelhaupt, F. M.; Bo, C.; Boerrigter, P. M.; Cavallo, L.; Chong, D. P.; et al. *Computer Code ADF 2015.01 SCM, Theoretical Chemistry*; Vrije Universiteit: Amsterdam, The Netherlands, 2015.
(29) te Velde, G.; Bickelhaupt, F. M.; Baerends, E. J.; Fonseca Guerra, C.; van Gisbergen, S. J. A.; Snijders, J. G.; Ziegler, T. Chemistry with ADF. *J. Comput. Chem.* **2001**, *22*, 931−967.
(30) Baerends, E. J.; Ellis, D. E.; Ros, P. Self-Consistent Molecular Hartree-Fock-Slater Calculations - I. The Computational Procedure. *Chem. Phys.* **1973**, *2*, 41−51.
(31) van Lenthe, E.; Baerends, E. J.; Snijders, J. G. Relativistic Total Energy Using Regular Approximations. *J. Chem. Phys.* **1994**, *101*, 9783−9792.
(32) Lee, C. T.; Yang, W. T.; Parr, R. G. Development of the Colle-Salvetti Correlation Energy Formula into a Functional of Electron Density. *Phys. Rev. B: Condens. Matter Mater. Phys.* **1988**, *37*, 785−789.
(33) Handy, N. C.; Cohen, A. J. Left-Right Correlation Energy. *Mol. Phys.* **2001**, *99*, 403−412.
(34) Bento, A. P.; Sola, M.; Bickelhaupt, F. M. Ab Initio and DFT Benchmark Study for Nucleophilic Substitution at Carbon (S_N2@C) and Silicon (S_N2@Si). *J. Comput. Chem.* **2005**, *26*, 1497−1504.
(35) Swart, M.; Sola, M.; Bickelhaupt, F. M. Energy Landscapes of Nucleophilic Substitution Reactions: A Comparison of Density Functional Theory and Coupled Cluster Methods. *J. Comput. Chem.* **2007**, *28*, 1551−1560.
(36) Bento, A. P.; Sola, M.; Bickelhaupt, F. M. E2 and S_N2 Reactions of X^- + CH_3CH_2X (X = F, Cl); an Ab Initio and DFT Benchmark Study. *J. Chem. Theory Comput.* **2008**, *4*, 929−940.
(37) Swart, M.; Sola, M.; Bickelhaupt, F. M. Density Functional Calculations of E2 and S_N2 Reactions: Effects of the Choice of Method, Algorithm, and Numerical Accuracy. *J. Chem. Theory Comput.* **2010**, *6*, 3145−3152.
(38) Gonzales, J. M.; Allen, W. D.; Schaefer, H. F. Model Identity S_N2 Reactions CH_3X + X^- (X = F, Cl, CN, OH, SH, NH_2, PH_2): Marcus Theory Analyzed. *J. Phys. Chem. A* **2005**, *109*, 10613−10628.
(39) Fan, L. Y.; Versluis, L.; Ziegler, T.; Baerends, E. J.; Ravenek, W. Calculation of Harmonic Frequencies and Harmonic Force Fields by the Hartree-Fock-Slater Method. *Int. J. Quantum Chem.* **1988**, *34*, 173−181.
(40) Fan, L.; Ziegler, T. The Application of Density Functional Theory to the Optimization of Transition-State Structures. 1. Organic Migration Reactions. *J. Chem. Phys.* **1990**, *92*, 3645−3652.
(41) Fukui, K. The Path of Chemical Reactions. The IRC Approach. *Acc. Chem. Res.* **1981**, *14*, 363−368.
(42) Ess, D. H.; Houk, K. N. Theory of 1,3-Dipolar Cycloadditions: Distortion/interaction and Frontier Molecular Orbital Models. *J. Am. Chem. Soc.* **2008**, *130*, 10187−10198.
(43) Ess, D. H.; Houk, K. N. Distortion/Interaction Energy Control of 1,3-Dipolar Cycloaddition Reactivity. *J. Am. Chem. Soc.* **2007**, *129*, 10646−10647.
(44) Bickelhaupt, F. M.; Baerends, E. J. In *Reviews in Computational Chemistry*; Lipkowitz, K. B., Boyd, D. B., Eds.; VCH: New York, 2000; Vol. *15*, pp 1−86.
(45) Ziegler, T.; Rauk, A. CO, CS, N_2, PF_3, and $CNCH_3$ as Sigma-Donors and Pi-Acceptors. Theoretical Study by the Hartree-Fock-Slater Transition-State Method. *Inorg. Chem.* **1979**, *18*, 1755−1759.
(46) Ziegler, T.; Rauk, A. A. Theoretical Study of the Ethylene-Ethylene-Metal Bond in Complexes between Cu^+, Ag^+, Au^+, Pt^0, or Pt^{2+} and Ethylene based on the Hartree-Fock-Slater Transition-State Method. *Inorg. Chem.* **1979**, *18*, 1558−1565.
(47) Bickelhaupt, F. M.; Nibbering, N. M. M.; VanWezenbeek, E. M.; Baerends, E. J. Central Bond in the 3 $CN^•$ Dimers NC-CN, CN-CN, and CN-NC. Electron Pair Bonding and Pauli Repulsion Effects. *J. Phys. Chem.* **1992**, *96*, 4864−4873.
(48) Bickelhaupt, F. M.; Diefenbach, A.; de Visser, S. P.; de Koning, L. J.; Nibbering, N. M. M. Nature of the Three-Electron Bond in H_2S Therefore SH_2^+. *J. Phys. Chem. A* **1998**, *102*, 9549−9553.
(49) Baerends, E. J.; Gritsenko, O. V. A Quantum Chemical View of Density Functional Theory. *J. Phys. Chem. A* **1997**, *101*, 5383−5403.
(50) van Zeist, W.-J.; Fonseca Guerra, C.; Bickelhaupt, F. M. PyFrag—Streamlining Your Reaction Path Analysis. *J. Comput. Chem.* **2008**, *29*, 312−315.
(51) Nibbering, N. M. M. Gas-Phase Ion Molecule Reactions as Studied by Fourier-Transform Ion-Cyclorton Resonance. *Acc. Chem. Res.* **1990**, *23*, 279−285.
(52) Wolters, L. P.; Bickelhaupt, F. M. Halogen Bonding versus Hydrogen Bonding: A Molecular Orbital Perspective. *ChemistryOpen* **2012**, *1*, 96−105.
(53) Pierrefixe, S. C. A. H.; van Stralen, S. J. M.; van Stralen, J. N. P.; Fonseca Guerra, C.; Bickelhaupt, F. M. Hypervalent Carbon Atom: "Freezing" the S_N2 Transition State. *Angew. Chem., Int. Ed.* **2009**, *48*, 6469−6471.
(54) Fonseca Guerra, C.; Handgraaf, J. W.; Baerends, E. J.; Bickelhaupt, F. M. Voronoi Deformation Density (VDD) Charges: Assessment of the Mulliken, Bader, Hirshfeld, Weinhold, and VDD Methods for Charge Analysis. *J. Comput. Chem.* **2004**, *25*, 189−210.
(55) Pauling, L. The Nature of the Chemical Bond. IV. The Energy of Single Bonds and the Relative Electronegativity of Atoms. *J. Am. Chem. Soc.* **1932**, *54*, 3570−3582.
(56) Pierrefixe, S. C. A. H.; Fonseca Guerra, C.; Bickelhaupt, F. M. Hypervalent Silicon versus Carbon: Ball-in-a-Box Model. *Chem. - Eur. J.* **2008**, *14*, 819−828.

DOI: 10.1021/acs.jpca.6b12240
J. Phys. Chem. A 2017, 121, 885−891